EPID-based verification of the MLC performance for dynamic IMRT and VMAT

Pejman Rowshanfarzad[a)]
School of Mathematical and Physical Sciences, University of Newcastle, Newcastle, NSW 2308, Australia

Mahsheed Sabet and Michael P. Barnes
Department of Radiation Oncology, Calvary Mater Newcastle Hospital, Newcastle, NSW 2310, Australia

Daryl J. O'Connor
School of Mathematical and Physical Sciences, University of Newcastle, Newcastle, NSW 2308, Australia

Peter B. Greer
Department of Radiation Oncology, Calvary Mater Newcastle Hospital, Newcastle, NSW 2310, Australia and School of Mathematical and Physical Sciences, University of Newcastle, Newcastle, NSW 2308, Australia

(Received 17 June 2012; revised 2 August 2012; accepted for publication 26 August 2012; published 24 September 2012)

Purpose: In advanced radiotherapy treatments such as intensity modulated radiation therapy (IMRT) and volumetric modulated arc therapy (VMAT), verification of the performance of the multileaf collimator (MLC) is an essential part of the linac QA program. The purpose of this study is to use the existing measurement methods for geometric QA of the MLCs and extend them to more comprehensive evaluation techniques, and to develop dedicated robust algorithms to quantitatively investigate the MLC performance in a fast, accurate, and efficient manner.
Methods: The behavior of leaves was investigated in the step-and-shoot mode by the analysis of integrated electronic portal imaging device (EPID) images acquired during picket fence tests at fixed gantry angles and arc delivery. The MLC was also studied in dynamic mode by the analysis of cine EPID images of a sliding gap pattern delivered in a variety of conditions including different leaf speeds, deliveries at fixed gantry angles or in arc mode, and changing the direction of leaf motion. The accuracy of the method was tested by detection of the intentionally inserted errors in the delivery patterns.
Results: The algorithm developed for the picket fence analysis was able to find each individual leaf position, gap width, and leaf bank skewness in addition to the deviations from expected leaf positions with respect to the beam central axis with sub-pixel accuracy. For the three tested linacs over a period of 5 months, the maximum change in the gap width was 0.5 mm, the maximum deviation from the expected leaf positions was 0.1 mm and the MLC skewness was up to 0.2°. The algorithm developed for the sliding gap analysis could determine the velocity and acceleration/deceleration of each individual leaf as well as the gap width. There was a slight decrease in the accuracy of leaf performance with increasing leaf speeds. The analysis results were presented through several graphs. The accuracy of the method was assessed as 0.01 mm for both the gap size and peak position determination.
Conclusions: This study provides fast, easy, and accurate test methods for routine QA of the MLC performance and helps in faster troubleshooting of MLC problems in both IMRT and VMAT treatments. © *2012 American Association of Physicists in Medicine*. [http://dx.doi.org/10.1118/1.4752207]

Key words: linac QA, MLC performance, VMAT, IMRT, EPID

I. INTRODUCTION

In intensity modulated radiation therapy (IMRT) treatments, nonuniform dose distributions of megavoltage beams are delivered to the patient in complex shapes. Intensity modulation is performed by means of motorized multileaf collimators (MLCs). Therefore, it is essential for patient safety to routinely monitor the MLC performance through strict quality assurance programs to ensure the accuracy and reproducibility of leaf motion in every fraction of the treatment plan.[1,2] In advanced radiotherapy treatments such as arc-IMRT (volumetric modulated arc therapy or VMAT), the QA of the collimation system may be more crucial, since doses could be delivered in more complex plans with the MLC shape, gantry speed, and dose rate changing during treatment in single or multiple gantry rotations.[3,4] In fact, it is rather challenging to provide appropriate techniques for the QA of linacs used for such sophisticated techniques.

Errors in MLC positioning may be either due to the inaccurate positioning of individual leaves or the result of systematic shifts in the leaf banks[5] or MLC carriage.[6] The accuracy of individual leaf positions may be affected by several factors including mechanical imperfections, gradual degradation of the performance of each motor,[2]

cable communication malfunctions,[7] and loss of counts by potentiometer encoders.[2] Leaves may slow down, get stuck, be misaligned, skewed, or be affected by inertia or gravity. In addition, the drive support assemblies could fail or have delay in communications with the MLC controller.[8,9] The MLC bank alignment during gantry rotation may be affected by gravity which causes drifts in the carriage drive and its supporting assemblies,[2,6,10] since they are heavy components and their weight could affect the window widths during gantry and collimator rotations.[2,6,9] Errors may also occur in the leaf calibration process[2,5,11,12] which are probably the main cause for systematic errors in leaf banks.[5,13]

Dosimetric consequences of systematic errors in leaf banks are reported to be proportional to the extent of errors and are more pronounced for treatments with small window openings.[5,14] Every 1 mm shift of the leaf banks has been predicted to result in 2.7% and 5.6% change in the reference equivalent uniform dose for prostate and head and neck fields, respectively.[5] In another study, Monte Carlo simulations have predicted ~6% dose difference as a result of 1 mm MLC systematic error in prostate step and shoot IMRT treatment plans.[14] An error of 1 mm in dynamic IMRT delivery with a window of 2 cm has been reported to cause 5% dose error.[15] However, measurements of the effect of 0.5 mm systematic offset in the leaves have shown up to 12% and 6% dose difference for head and neck and prostate fields, respectively.[16]

Budgell *et al.*[17] have shown that accurate dose delivery for IMRT fields requires better than 1 mm accuracy in leaf positioning. The AAPM Task Group report 142 recommends ±1 mm as the MLC positioning tolerance[18] while the ESTRO guidelines propose ±0.5 mm as the acceptance criterion.[19]

Different devices have been used for the QA of MLC leaves for IMRT/VMAT delivery. The conventional method for two-dimensional (2D) checking of MLC leaf positions was to use film images of a dynamic MLC (DMLC) leaf pattern.[13,20–24] Film images were either visually inspected or scanned, digitized, and contrast enhanced.[2] Visual inspection is a subjective and inaccurate method for checking the leaf pair alignment and uniformity of the gap widths. Using the scanned films is a better option but it is time-consuming and labor-intensive.[12,25–27] Another disadvantage of films is their pixel to pixel noise.[28]

Electronic portal imaging devices (EPIDs) provide images in digital format which can be used to quickly provide the image data required for analysis. They are easy to use and have a similar level of sensitivity as films for MLC QA applications while their imaging speed can be adjusted to catch up with the leaf motion.[12] Therefore, EPIDs were considered as more efficient alternatives to films, allowing the test to be performed more frequently.[2,12,15,27,29] EPIDs have been used for the QA of MLC performance in several studies.[7,9,15,25–27,30–33] There have also been reports on the application of 2D array detectors such as MapCheck, MatriXX, and PTW-729[34,35] for this purpose. The major concern about these devices is their low spatial resolution.

Another method for the QA of MLC leaves would be to use the dynamic log files (or Dynalog files) created at the end of each IMRT delivery by the Varian MLC controller software. Dynalog files have been tested[34] and used as reference in many studies on the leaf positioning accuracy.[8,22,23,36–38] However, the validity of the data in Dynalog files strongly depends on the accuracy of leaf position readouts. Any possible drift in the encoder readings could be temporarily improved by the MLC re-initialization,[9] but it must be routinely checked by independent imaging methods.[8,10]

Accurate delivery of a dynamic IMRT/VMAT treatment requires not only accurate leaf positioning, but also correct leaf speeds.[15] The leaf speed and its acceleration/deceleration should be investigated since they could affect the beam delivery and lead to artifacts in the beam intensity profile.[20,25,39] The MLC leaf positioning error is reported to be proportional to the leaf speed.[22] Investigation of the stability of MLC has been performed by film imaging[20] or looking at the MLC log files at cardinal angles.[39]

In the present study, some important MLC characteristics during IMRT/VMAT deliveries have been examined, and reliable QA techniques for MLC leaves have been implemented based on some popular test patterns that have already been accepted and used worldwide. The elements which have been quantitatively investigated in this work include: (a) the accuracy and stability of each individual MLC leaf position and their resulting gap widths; (b) the skewness of leaf banks/carriage; (c) the speed of each leaf over the whole range of its positions; and (d) the acceleration/deceleration of each individual leaf. These items have either not been studied in previous studies or not been measured with this level of accuracy. The study is based on the acquisition of EPID images in integrated and cine imaging modes and development of robust and highly accurate codes to automatically analyze the image data. Finally, a large amount of useful information on the behavior of MLC leaves is presented in an efficient manner. The ultimate aim of this study is to develop and implement faster and more accurate QA techniques for MLC leaves in both dynamic and arc IMRT deliveries.

II. METHODS AND MATERIALS

II.A. Materials

A Varian trilogy linear accelerator (Varian Medical Systems, Palo Alto, CA) operating in the 6 MV photon mode was used for all irradiations. The linac was equipped with Millennium™ 120 leaf MLC, which includes two banks (A and B) each with 60 tungsten alloy round-ended leaves mounted on a carriage. The 40 central leaves in each bank are 0.5 cm thick (at the isocenter level) and are called inner leaves. The peripheral 20 leaves are 1.0 cm thick and are called outer leaves. Each leaf is equipped with a motor which is driven by the MLC controller and drives the leaf along the carriage. The leaf extension range is 14.5 cm at the isocenter level. Further leaf motions require the movement of the carriage. The maximum leaf speed is 3 cm/s.

Megavoltage images were acquired with an aS1000 EPID attached to the linac by an E-type supporting arm. The active area of the imager was a 40 × 30 cm^2 matrix containing 1024 × 768 pixels. The method developed in this study was

tested on three other Varian linacs equipped with Millennium 120 leaf MLC and aS500 EPIDs with detector arrays of 384 × 512 pixels. EPID images were acquired in DICOM format and were automatically dark-field and flood-field corrected by the imaging system software. The gantry angles were set according to the IEC convention.[40] Data analysis and algorithm development were carried out using the MATLAB programming language and software (The Mathworks Inc., Natick, MA) in a PC with 3.10 GHz CPU and 4.0 GB RAM.

II.B. Measurement methods

II.B.1. Accuracy of leaf positioning

The leaf pattern used for the investigation of geometric accuracy and the reproducibility of positioning for each individual leaf was defined by leaf pairs moving across the field forming a sliding slit which was stopped at a number of equally spaced positions yielding narrow hot spots. This pattern was first introduced by Chui *et al.*[20] and has since been widely used and well known as the picket fence pattern. In this work, for measurements at fixed gantry angles, slits of 2 × 20 cm^2 dimensions stopping every 2 cm were used to produce seven pickets. For measurements in arc mode, 10 pickets of 0.1 × 20 cm^2 size were formed by a sliding gap (dMLC) stopping at 1.5 cm intervals. The test was performed in both conditions to cover the QA method for both IMRT and VMAT deliveries.

For fixed-gantry conditions, the EPID was positioned at 150 cm source to detector distance (SDD), the collimator angle was set to zero, and the jaws were parked at X = 18 cm and Y = 20 cm. The test with fixed gantry was repeated at cardinal angles to maximize the gravity effect at 90° and 270°.

The picket fence pattern explained above for fixed-gantry conditions was also used with the jaws parked at X = 20 cm and Y = 40 cm, the EPID at SDD = 100 cm and the collimator angle was set to 90°. Thus, all MLC leaves were included in the test. The gantry was fixed at zero angle. EPID images were acquired in integrated mode during the delivery of 100 MU beams at a rate of 300 MU/min.

For the experiments in the arc mode, the EPID was positioned at SDD = 105 cm and the jaw-defined field size was 20 × 20 cm^2. The linac was running at a nominal dose rate of 600 MU/min delivering 480 MU during a 352° gantry rotation. The test pattern for arc mode was based on the pattern introduced by Ling *et al.*[22] It was provided by Varian Medical Systems and was available via myVarian homepage.[41] All plans were imported into the ECLIPSE™ treatment planning system, and scheduled and measured through the ARIA® information system. EPID images were saved in ARIA and exported in DICOM format. The angular dependency of MLC performance can also be checked with this test.

An algorithm was developed which provided four main outputs from the picket fence test, including: (a) the deviation of the peak position of each individual leaf pair from the average of all peak positions in the picket, which shows the error for each leaf pair; (b) the deviation of each actual peak position from its expected position (with respect to beam central axis), which reveals any systematic shift in leaf positioning; (c) the distance between opposing leaves (gap width) for each individual leaf pair; and (d) the skewness of leaf banks/carriage and differentiating it from the collimator misalignment and EPID rotation in its plane.

In order to check the effect of EPID and gantry sag on the picket fence test results during arc deliveries, cine EPID images acquired during the delivery were corrected based on the method introduced in a previous study[42] using the sag pattern for the system under test. The corrected and uncorrected cine images were separately added up and their picket fence test results were compared. The effect of EPID sag in the beam direction on gap size was less than 0.003 mm and the combined effect on the gap size of EPID sag in its plane plus the gantry sag was found to be less than 0.06 mm. These values were negligible and were not corrected in the algorithm.

Furthermore, picket fence images acquired immediately after initialization and after 4 h of using the linac were compared to investigate the effectiveness of reinitializing the MLC.

II.B.2. Dynamic MLC performance

Although the leaf positioning can be investigated by the picket fence test, it cannot provide sufficient information on all aspects of the MLC system performance, since it can only give the data for certain points where the sliding gap stops. To verify the stability of leaf speed in a dynamic IMRT/VMAT delivery and the acceleration and deceleration of leaves as well as investigation of the consistency of gap width, a 0.5 × 20 cm^2 MLC-defined slit was moved across a 14 × 20 cm^2 field. The linac was running at a dose rate of 600 MU/min and both the collimators and gantry were at zero degrees for the fixed-gantry measurements. The EPID was positioned at SDD = 150 cm and images were acquired in cine mode using the IAS3 software (version 7.3.15).

The image acquisition time was set to 133.3 ms by capturing only one frame per image (7.5 frames per second). The slit was moved through five different patterns to comprehensively test the leaf performance step by step in various possible conditions:

(a) Unidirectional, starting from one end of the field and stopping at the other end, traveling with a constant speed with the gantry fixed at zero degree. Using different monitor units for this test led to a range of leaf speeds from 6.7 to 29.0 mm/s. The test was repeated at cardinal angles to investigate the angular dependence of the leaf speed and the gap width. In addition, it was repeated at 90° collimator angle (zero gantry angle) with a wider field to include the outer leaves and to investigate the consistency of the dynamic properties of the inner and outer leaves.
(b) Unidirectional, starting from one end of the field and stopping at the other end, traveling with a constant speed in an entire 360° gantry rotation with the collimator at zero angle. Using 360 MU irradiations led to a nominal leaf speed of 2.0 mm/s.

(c) Starting from one end of the field and stopping at the other end, returning to the start point with the same constant speed with the gantry fixed at zero degree. Application of 150 MU provided a nominal leaf speed of 19.3 mm/s.

(d) Unidirectional, starting from one end of the field and stopping at the other end, traveling in five sequences of uniform motion each with a different speed with the gantry fixed at zero degree. A range of dose fractions were used for similar distances to provide different leaf speeds for each sequence ranging from about 2 mm/s to 20 mm/s.

(e) Finally, a wider sliding gap (14×20 cm^2) was used from an acceptance test plan provided by Varian (dynamic arc leaf speed test). The gap width was 14 cm and moved across a large 28×20 cm^2 field to and from one side to the other. Ten oscillations were made while the gantry rotated from 90° to 270°. Thus, an overall distance of 140 cm was covered. The collimator was set at zero angle. Measurements were performed using 500 MU which led to a nominal leaf speed of 27.5 mm/s.

All MLC-defined fields for this study were generated using the commercial MLC Shaper software (version 6.3, Varian Medical Systems Inc., Palo Alto, CA). The speed of each individual leaf was determined in addition to the width of the sweeping gap for each test. The stability of leaf speeds in each sequence of test (d) was assessed. The last test was used to investigate the acceleration and deceleration of each leaf, since the speed gradients were larger.

The gantry and EPID sag effects were not considered for the sliding gap tests in arc mode, since cine EPID images were acquired every ~0.7° and the sag effect would be negligible in such a small angle and short duration of time.

II.B.3. Data processing

II.B.3.a. Picket fence analysis algorithms. An algorithm was developed to detect the position of each individual leaf from the picket fence images. The steps followed in the algorithm are briefly explained below.

(1) The image borders were determined based on 50% of the signal on the central cross-plane and in-plane profiles [points U, D, L, and R in Fig. 1(a)].

(2) A profile was plotted in the in-plane direction through the left border between the upper and lower borders [dotted line (P_L) in Fig. 1(a)].

(3) A Fourier first harmonic curve was fitted through the data points of the profile (P_L) to find the spatial frequency of leaf positions [k in Fig. 1(b)]. The spatial frequency for the outer leaves was twice that of the inner leaves and this was considered by automatic determination of the field length.

(4) The Canny edge detection filter[43] was applied to the image [Fig. 1(c)] to roughly find the position of leaves and the area between each two pickets (sub-areas A_1 to A_6). It must be noted that different edge detection

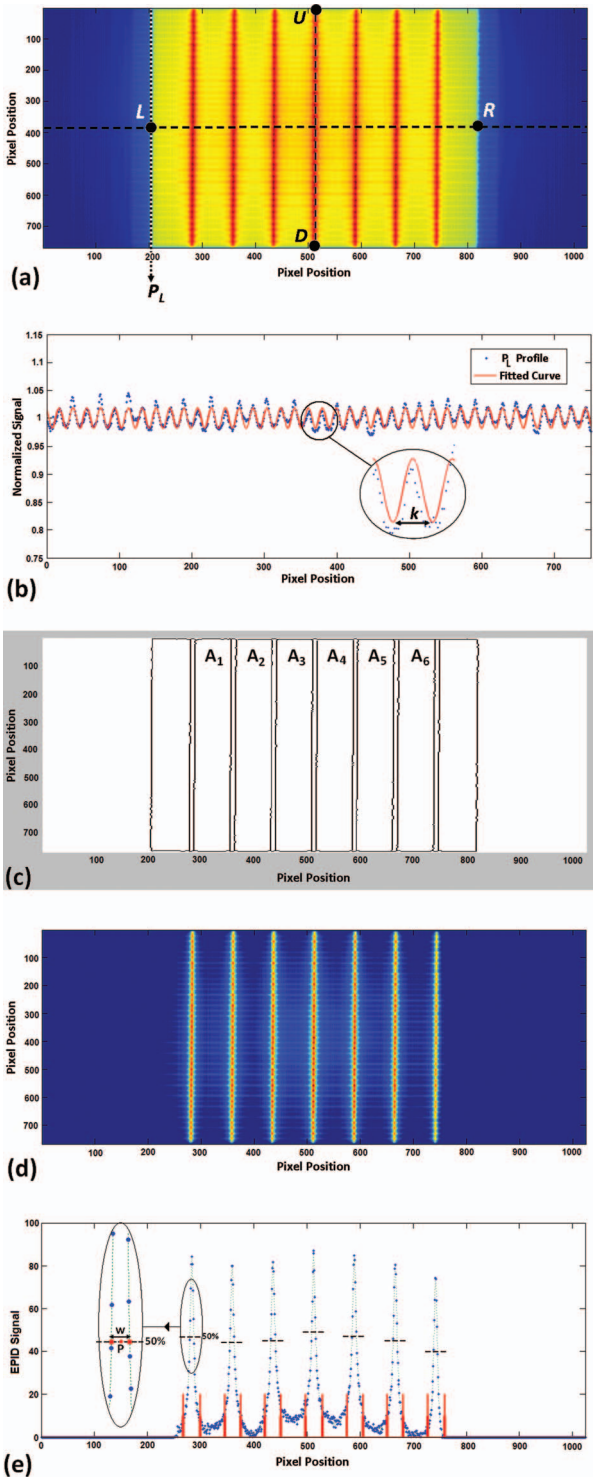

FIG. 1. Illustration of the main steps of the algorithm used for analysis of the picket fence images: (a) determination of image borders (U, D, L, and R), a profile (P_L) is passed through the left border; (b) fitting the first Fourier harmonic curve through the data points of (P_L) and finding the spatial frequency (k) of the leaves; (c) application of the Canny filter and determination of the edges in the image; (d) subtraction of the background signal from the image to increase the contrast; and (e) a sample profile passed through one leaf in the cross-plane direction. The vertical bars are results of the Canny filter with additional offsets in both left and right directions to include the full width of the picket. They are used to define the region of interest to find the 50% of signal for each picket. The horizontal dashed lines indicate the position of the 50% signal level for each picket. The peak position (P) and the gap width (w) are shown on the magnified picket on the left.

filters were tested for detection of the leaf positions and the Canny filter was found to be the optimum technique for this purpose.

(5) The mean pixel value for each sub-area was determined and their minimum was subtracted from the whole image matrix to eliminate the background and increase the image contrast [Fig. 1(d)].

(6) Using the leaf positions found in step (3), cross-plane profiles were plotted through each leaf. The average of five cross-plane profiles was used for the analysis. Depending on the MLC pattern measured (fixed-gantry or arc), a certain number of peaks should be observed on the profiles [dotted curves in Fig. 1(e)].

(7) Based on a previously developed algorithm already explained in detail in other publications,[6,42,44] the position of the 50% value of the intensity profile on the left and right edges of the peaks were determined with sub-pixel accuracy [Fig. 1(e)].

(8) The distance between the right and left edges of each peak (the full width at half maximum or FWHM) gives the gap widths [w in Fig. 1(e)], and their mean position indicates the peak position with sub-pixel accuracy [point (P) in Fig. 1(e)].

The measured position of each peak was compared with its expected position to find any possible systematic shift. The pixel positions were calibrated to absolute coordinates relative to the center of the beam on the EPID (CAX). This point which was used as reference has already been determined using a simple method explained in the literature[45,46] and was read out from a text file.

(9) Considering the SDD and EPID resolution, all results were automatically scaled to millimeter distances at the isocenter level.

(10) A line was fitted through the peak positions along each picket. If the lines were not vertical, the skewness of the system was determined from the slope of the lines (α). To differentiate between the leaf bank skewness relative to the collimator and the effects of collimator angle misalignment and EPID rotation in its plane, the Radon transform[47] was applied to one of the subareas between the pickets [e.g., A_3 in Fig. 1(c)] to determine the orientation of interleaf leakages (β). The resulting angle was subtracted from (α) and gives the net skewness of the leaf bank (θ). All MLC positions were subsequently corrected for the determined angle misalignment (α).

(11) The results were automatically illustrated in five separate graphs showing:

- The gap width for each leaf pair: if the gap width violates the accepted range for tolerance (± 1 mm),[18] the corresponding position was flagged.
- The angle of skewness for each picket (θ).
- The peak positions for each leaf pair relative to their average over each picket.
- The peak positions for each leaf pair relative to their expected positions.
- Three histograms showing the percentage frequency of: deviations from the average, deviations from the expected positions, and the distribution of the gap widths.

(12) The data presented in the graphs for each leaf were also automatically saved in the form of a text file in the folder which contains the DICOM images. The file is named as the date of the test and known as the picket fence log file. Having access to the log files from different dates would be useful for future reference.

It must be noted that the SDD and date of the test were read out from the DICOM image headers, and the EPID resolution (aS1000/aS500) and the collimator angle (0°/90°) were automatically determined in the algorithm by finding the matrix size and image profile characteristics after the Canny filter is applied.

II.B.3.b. Analysis algorithm for the sliding gap images. Another algorithm was developed to analyze each individual image acquired in cine mode during the delivery of sliding gap patterns. The steps followed in the algorithm are briefly explained below:

(1) The first three steps were similar to the algorithm for the picket fence analysis [steps (1)–(3) in Sec. II.B.3.a].

(2) Using the leaf positions obtained from the Fourier fit, cross-plane profiles were plotted along the centerlines of the leaves. The average of five cross-plane profiles was used for each leaf to improve the statistics. Only one peak was expected on each profile.

(3) Based on the method shown in Fig. 1(e), the position of the left and right gap edges (and subsequently the gap width) were determined individually for each leaf. The movements of the leaves during each frame acquisition are not expected to affect the accuracy of gap width determination, since the leaf pairs travel simultaneously with the same speed in the same direction. The distances were converted into millimeters and back-projected to the isocenter level.

The above processes were executed as a core function for each individual image in a series of cine acquisitions, and the data extracted from each single image were automatically stored in separate vectors, each including the data for all leaves that form the gap. The vectors were concatenated to form matrices of data (e.g., gap widths) with rows containing the data for each leaf pair. The number of matrix rows and columns were equal to the number of leaves and the number of cine images, respectively.

(4) A correction was applied in the code for the known effect of rounded leaf edges[48–51] based on the leaf position offset file (MLCTABLE.txt) provided by Varian for geometric corrections.

(5) The number of frames and applied dose rates (300 or 600 MU/min) were readout from the DICOM header. These were used for determination of the time for acquisition of each image (t) that is equal the num-

ber of frames divided by the frame acquisition rate (which is 6.67 s^{-1} for 300 MU/min, and 7.50 s^{-1} for 600 MU/min dose rate).

(6) The speed of each leaf was determined using the leaf positions in each two consecutive images and the time (t).

(7) The acceleration/deceleration of each leaf was found in a similar manner to step (5).

(8) The results were automatically illustrated in separate figures showing:

- The gap width for each leaf pair versus position while crossing the field; if the gap width was outside the accepted tolerance of ±1 mm from the planned width, a red bullet appeared beside the figure, otherwise the bullet was green. [Figures 3(a) to 7(a)].
- The deviation of gap widths from the average of gap widths defined by the corresponding leaf pair across the field (this quantifies the behavior of each leaf pair separately).
- Two figures showing the leaf speeds versus position while crossing the field for each leaf bank separately; if the leaf speed was out of the accepted tolerance of ±5 mm/s from the planned speed,[18] a red bullet appeared beside the figure, otherwise the bullet was green. [Figures 3(c) and 3(d) and 4(c) and 4(d)].
- Two figures showing the leaf acceleration/deceleration at different positions while crossing the field for each leaf bank separately.

(9) The data presented in the figures for each leaf were also automatically saved in the form of a text file in the folder which contained the DICOM images. The file was named as the date of the test and known as the sliding gap log file. Having access to the log files from different dates would be useful for future reference.

II.B.4. Accuracy of the algorithm

Intentional known errors were inserted in a number of leaf positions in the picket fence pattern by applying a range of displacements from 0.1 to 2.5 mm to the gap width (at the isocenter level), and also by changing the gap position in randomly selected leaf pairs without modification of the gap width. The ability of the algorithm to detect these errors could indicate its level of accuracy. Each measurement was repeated three times to reduce the uncertainties.

The accuracy of MLC skewness detection depends on the accuracy of the Radon transform. The latter was tested by rotating the image by different angles in a range of 0.1°–1° at 0.1° intervals and detecting the angles by the Radon transform method.

III. RESULTS

III.A. MLC positioning

A series of graphical outputs produced by the algorithm is shown in Fig. 2 for a picket fence test with intentional errors of 0.5 mm, 1.0 mm, and 1.5 mm in the gap width of pickets 5, 6, and 7. Figure 2(a) shows the EPID image from step (5) of Sec. II.B.3.a to provide a visual illustration of the leaf positions. In this figure, the two orthogonal lines through the center of radiation field (CAX) in the in-plane and cross-plane directions are automatically plotted to help visual detection of any systematic shifts in the leaf positions. Figure 2(b) includes a series of graphs showing the gap widths for each individual leaf pair in all pickets. The deviations of peak positions from their average and from their expected positions (with respect to beam central axis) are plotted for each leaf pair in Figs. 2(c) and 2(d), respectively. The points where deviations are larger than the tolerance limit are automatically flagged by the error value and the corresponding leaf number (leaves 16 and 21 in pickets 6 and 7, respectively). In cases where errors are detected in peak positions, the flags will appear on graphs (c) and (d). If such results appear in routine tests, the corresponding leaves are considered out-of-range and investigation would be required. It should be noted that the 0.5 mm intentional error in picket 5 has not triggered a flag, since it is within the tolerance level. The total skewness of the system measured for all pickets at each leaf position is shown in Fig. 2(e). The average skewing of the system and the MLC bank alone are given in the graph title. Finally, three histograms are generated in Fig. 2(f) which statistically summarize the data in Figs. 2(b)–2(d).

The maximum time required to perform each measurement was less than 2 min and the data processing required less than 15 s for all tests.

The picket fence test was performed on all tested linacs for 5 months and the results of MLC performance investigations are summarized in Table I.

The picket fence test was repeated (three times) with the collimator at 90° to include all MLC leaves. The results showed that for the outer leaves, the average gap width was 0.01 ± 0.00 mm larger than the average gap width of the inner leaves and the average peak position was 0.08 ± 0.00 mm displaced from those of the inner leaves.

The picket fence test results were compared after the MLC initialization and 4 h later. The results showed a shift in the peak position of up to 0.1 mm and 0.2 mm for 2% and 1% of the 420 data points, respectively. The change in the gap widths was up to 0.1 mm for 3%, 0.2 mm for 3.5%, 0.3 mm for 5% and 0.4 mm for 0.5% of the data points.

III.B. Dynamic MLC performance

Several measurements of the MLC speed, variations of the gap width, and leaf acceleration/deceleration were carried out using cine EPID images acquired during sliding gap deliveries. A sample of each set of the algorithms outputs is given in this section. Similar types of graphical outputs are presented in Figs. 3–7 for a number of different measurement conditions. Figures 3 and 4 are the result sheets for a unidirectional crossing gap moving with a constant speed for both the fixed-gantry measurements (∼10 mm/s), and arc mode (∼2 mm/s). Another sliding gap starting from one end of the field and stopping at the other end, returning to the start

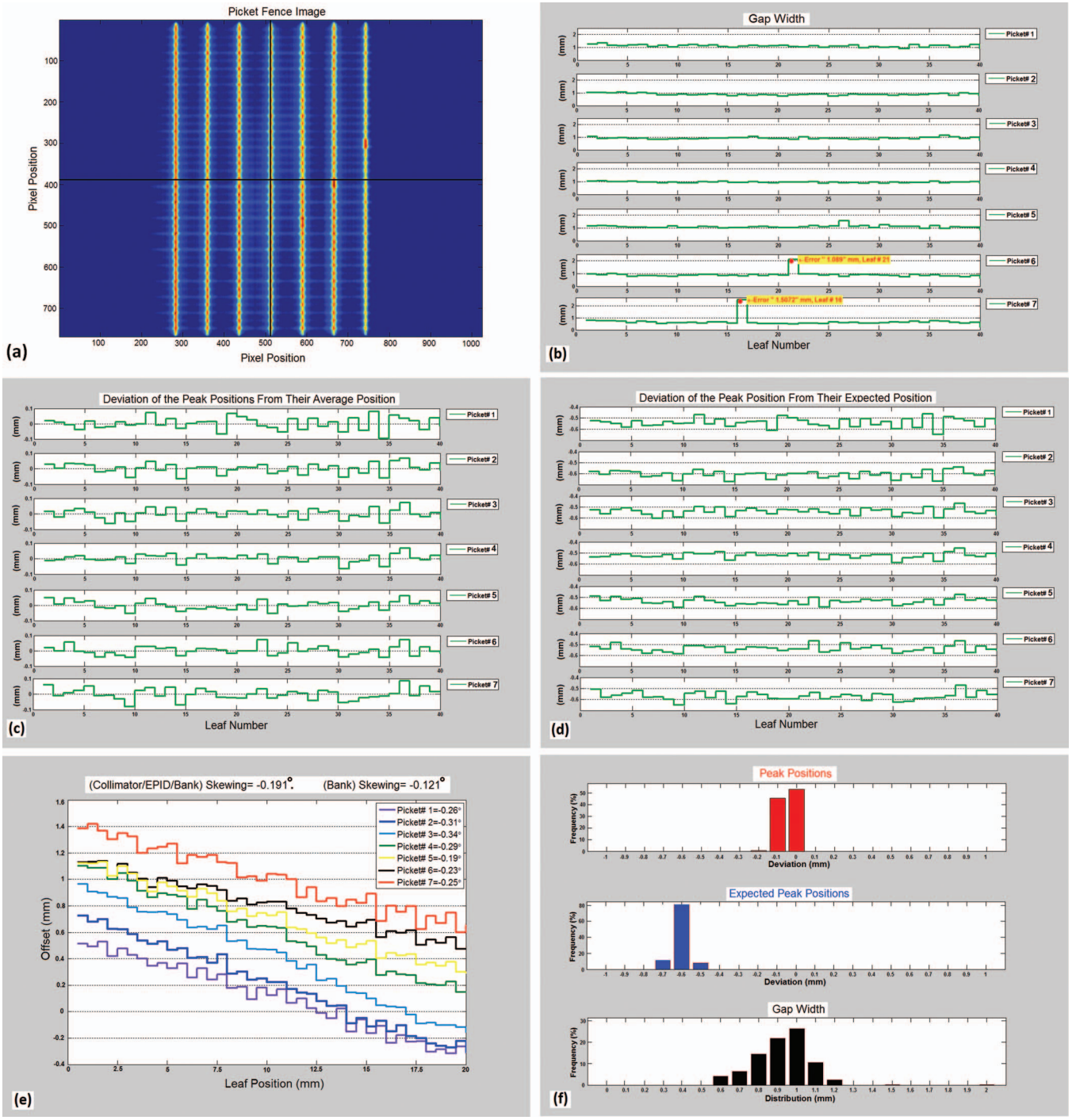

FIG. 2. The graphs automatically produced by the algorithm for the picket fence test analysis including 0.5, 1.0, and 1.5 mm intentional errors inserted in the gap width in leaves 26, 21, and 16 at pickets 5, 6, and 7, respectively: (a) the improved EPID image; (b) the gap width for each individual leaf at all pickets including flags for the out-of-range gap widths (leaves 21 and 16 in pickets 6 and 7); (c) deviation of peak positions from their average in each picket; (d) deviation of peak positions from their expected positions in each picket; (e) skewness of the system at each picket; and (f) histograms of the peak positions, expected peak positions and the gap width distribution.

point with the same constant speed is analyzed in Fig. 5. Results for a unidirectional gap traveling with different but uniform speeds are shown in Fig. 6, and finally the analysis for an oscillating sliding gap during arc delivery is shown in Fig. 7. There are four components (a)–(d) in each of these figures:

(a) shows the gap width at all different positions/gantry angles/delivery times across the field for each individual leaf pair depending on the measurement condition;

(b) illustrates the deviations of gap widths from the average of gap widths defined by the corresponding leaf pair across the field;

TABLE I. Results of the picket fence algorithm on three linacs over 5 months. The average of the maximum deviations measured at each session is presented ±1 SD for each linac. The nominal gap width was 1 mm.

Tested linac	# 1	# 2	# 3
Maximum gap width (mm)	1.52 ± 0.14	1.48 ± 0.20	1.23 ± 0.15
Maximum deviation from average peak position (mm)	0.12 ± 0.04	0.09 ± 0.02	0.09 ± 0.02
Maximum deviation from expected peak position (mm)	0.80 ± 0.07	0.56 ± 0.06	0.17 ± 0.04
Maximum MLC skewness (degrees)	0.16 ± 0.03	0.04 ± 0.01	0.07 ± 0.02

(c) and (d) show the speeds of the left and right MLC banks at each individual leaf position/gantry angle/delivery time, respectively. Similar patterns are expected for the left and right banks.

The oscillating gap test was a suitable case to investigate the leaf acceleration/deceleration due to the hysteresis resulting from moving the leaves back and forth. Therefore, two more graphs (e) and (f) are added in Fig. 7 to show the acceleration/deceleration of each leaf for different gantry angles. According to these graphs, the leaves had consistent speeds in each sequence with narrow junctions which indicate rapid changes in the leaf direction, as expected.

The presence of hot or cold spots on any of the above patterns could be the result of inconsistencies in the leaf speeds. Figures 3, 5, and 6 each represent the data from more than 4100 points, while the number of data points included in Figs. 4 and 7 are 21 400 and 14 250, respectively.

The maximum time required to perform each measurement was less than 2 min and the data processing required less than 20 s for the tests at fixed gantry angles. The results for the arc mode including the unidirectional sliding gap and the oscillating gap test took 60 s and 90 s to process, respectively.

III.C. Comparison of the results of DMLC tests

A unidirectional sliding gap delivered at a fixed gantry angle was tested for four different leaf speeds and the results of their statistical analysis are summarized in Table II. The

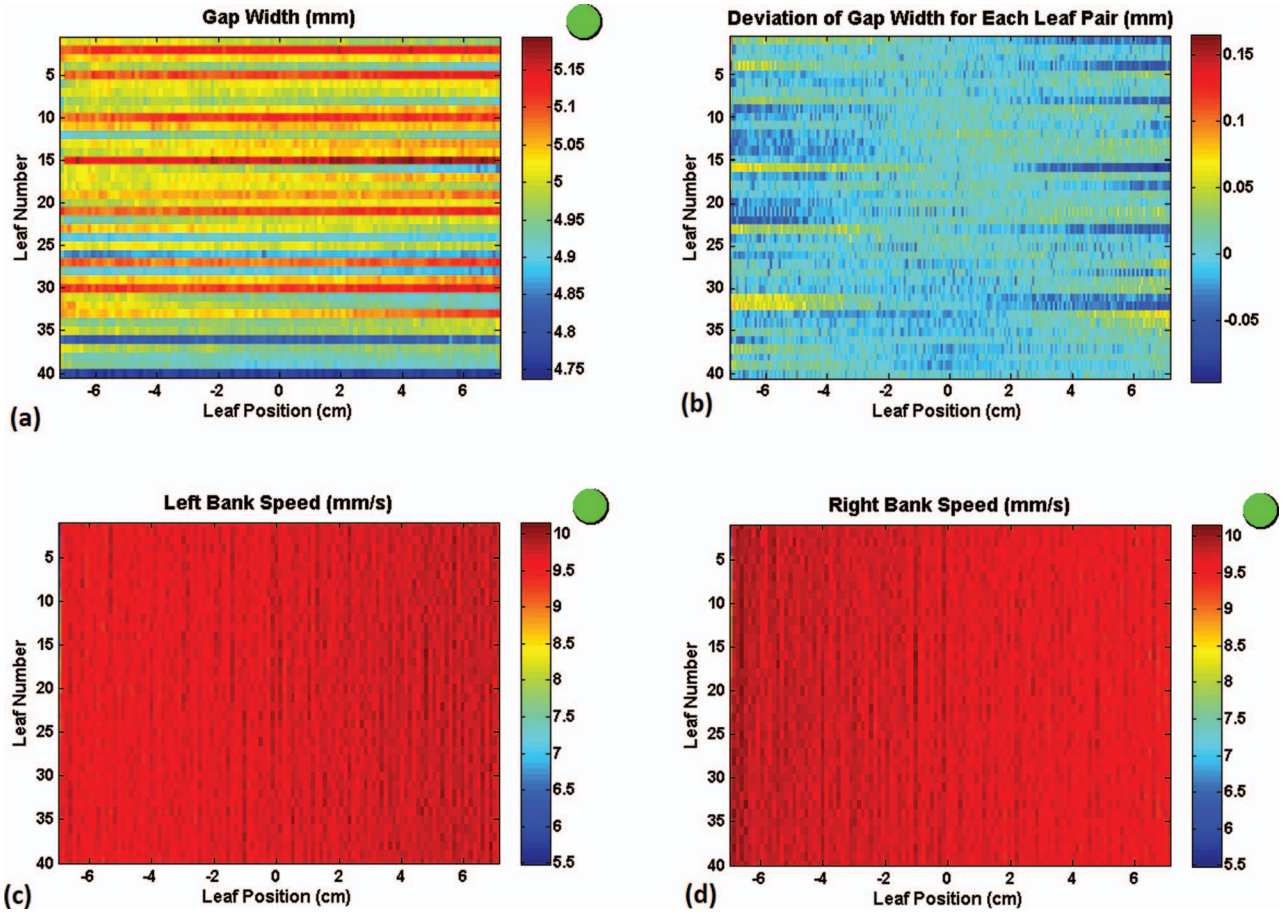

FIG. 3. The graphical output sheet for the analysis of a unidirectional 5 mm sliding gap with a constant speed of ~10 mm/s using a fixed gantry angle: (a) the gap width pattern for different leaf positions across the field; (b) deviation of the gap widths from the average of gap widths defined by the corresponding leaf pair across the field; (c) the speed of each leaf in the left bank; and (d) the speed of each leaf in the right bank.

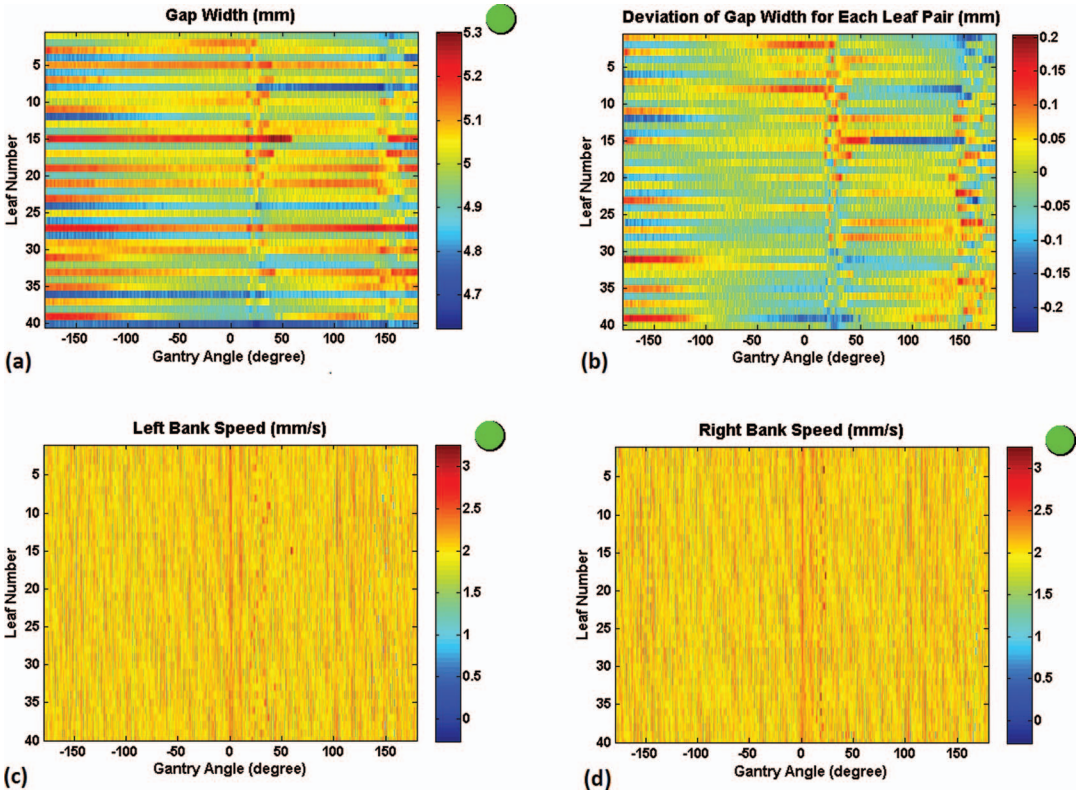

FIG. 4. The graphical output sheet for the analysis of a unidirectional 5 mm sliding gap with constant speed (~2 mm/s) delivered during an entire 360° arc: (a) the gap width versus gantry angle; (b) deviation of the gap widths from the average of gap widths defined by the corresponding leaf pair across the field; (c) the speed of each leaf in the left bank; and (d) the speed of each leaf in the right bank.

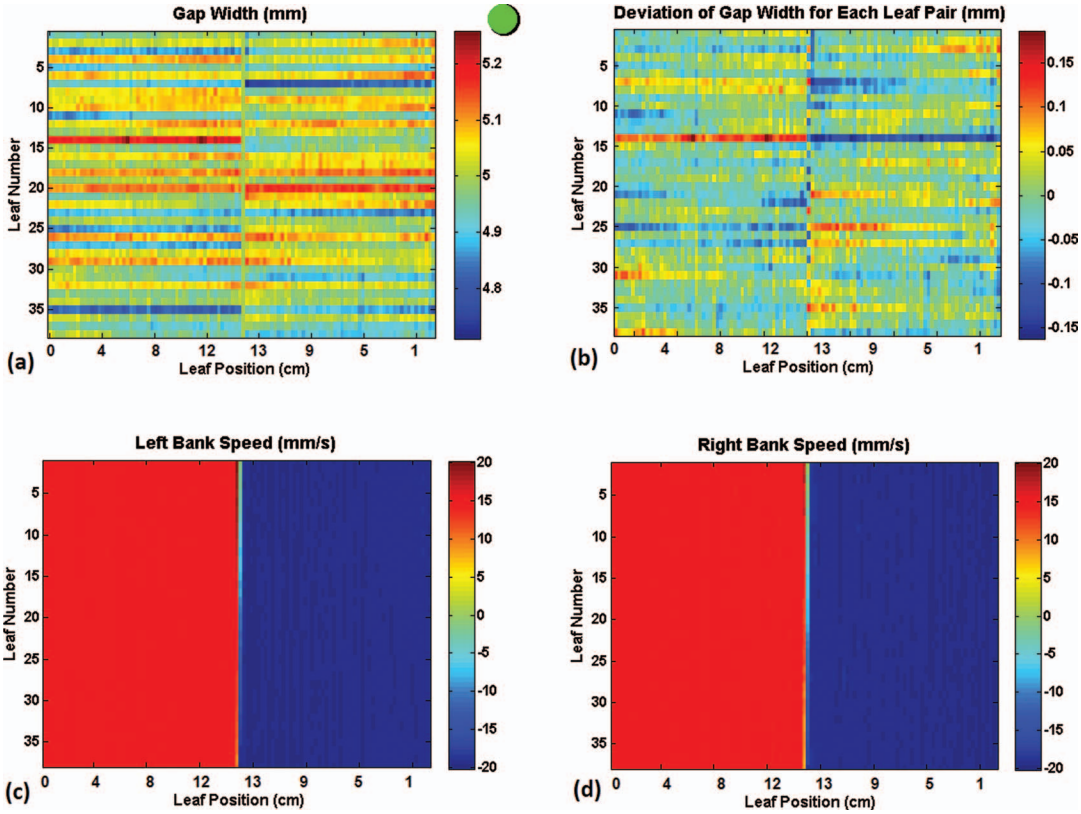

FIG. 5. The graphical output sheet for the analysis of a 5 mm sliding gap traveling with constant speed (~19 mm/s) across the field from one end to the other and returning to the original position using a fixed gantry angle: (a) the gap width pattern for different leaf positions across the field; (b) deviation of the gap widths from the average of gap widths defined by the corresponding leaf pair across the field; (c) the speed of each leaf in the left bank (left to right movement is considered as the positive direction); and (d) the speed of each leaf in the right bank.

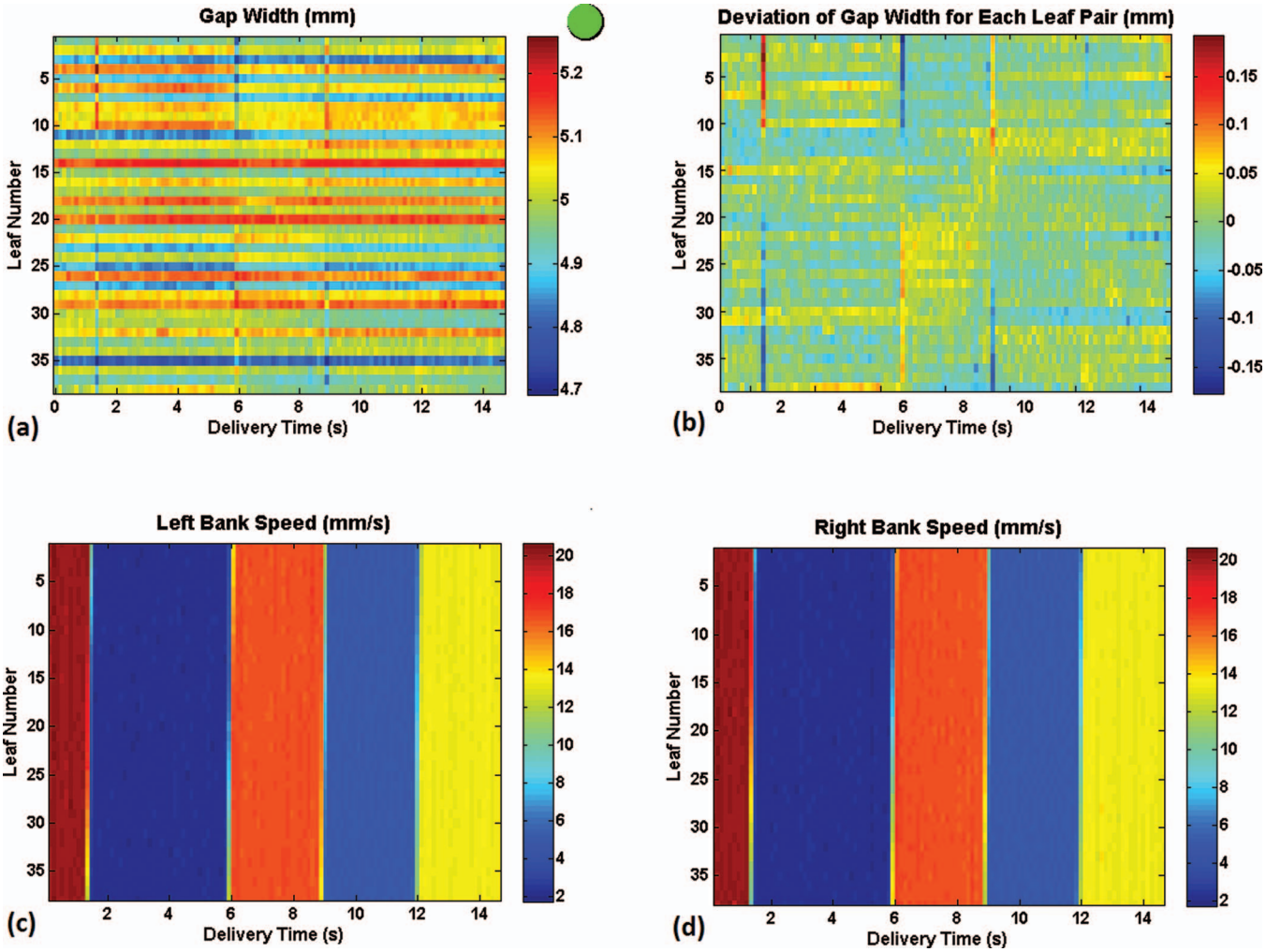

FIG. 6. The graphical output sheet for the analysis of a 5 mm sliding gap traveling across the field in five sequences each with a different constant speed (20.1, 2.2, 16.7, 5.0, and 13.4 mm/s from left to right) using a fixed gantry angle: (a) the gap width pattern for different delivery times across the field; (b) deviation of the gap widths from the average of gap widths defined by the corresponding leaf pair across the field; (c) the speed of each leaf in the left bank; and (d) the speed of each leaf in the right bank.

change in leaf speed was achieved by applying a different number of monitor units. The average detected and nominal leaf speeds were compared for each experiment, and the maximum deviation of the detected leaf speeds (among all leaf positions) from the global average are listed for each measurement. The root mean square deviation (RMSD) between the leaf speeds at corresponding positions in the left and right banks are calculated. In addition, the gap widths have been investigated for all leaf pairs by looking at their maximum deviation from the nominal gap width (5 mm) across the field, and by evaluation of the RMSD of the measured and nominal gap widths at all positions across the field.

Table II shows that there is a slight decrease in the accuracy and precision of leaf performance with increasing leaf speed.

The unidirectional sliding gap delivered at a fixed gantry angle was also repeated at 90° collimator angle to include the outer leaves (only for the 9.67 mm/s leaf speed). The results showed that the inner and outer leaves had the same speeds, while the average gap width for the outer leaves was 0.24 ± 0.32 mm larger than the inner leaves.

Results of the other experiments on leaf speed and acceleration/deceleration are summarized in Table III. The RMSD of the measured and nominal gap widths for all leaf positions/gantry angles are presented along with the maximum difference between the measured and nominal gap widths and the RMSD between the measured speeds for corresponding leaves in the left and right banks.

Tables II and III provide detailed data for comparison of several different leaf performance conditions. The arc delivery data showed larger deviations due to the gravity effect.

III.D. Angular dependence

The picket fence test results measured at cardinal angles and during arc delivery are compared in Table IV. The data are averaged over all leaf pairs and picket positions, and are given ± 1 SD. The number of data points were (40 × 7 = 280) for the fixed-gantry measurements and (40 × 10 = 400) in arc mode.

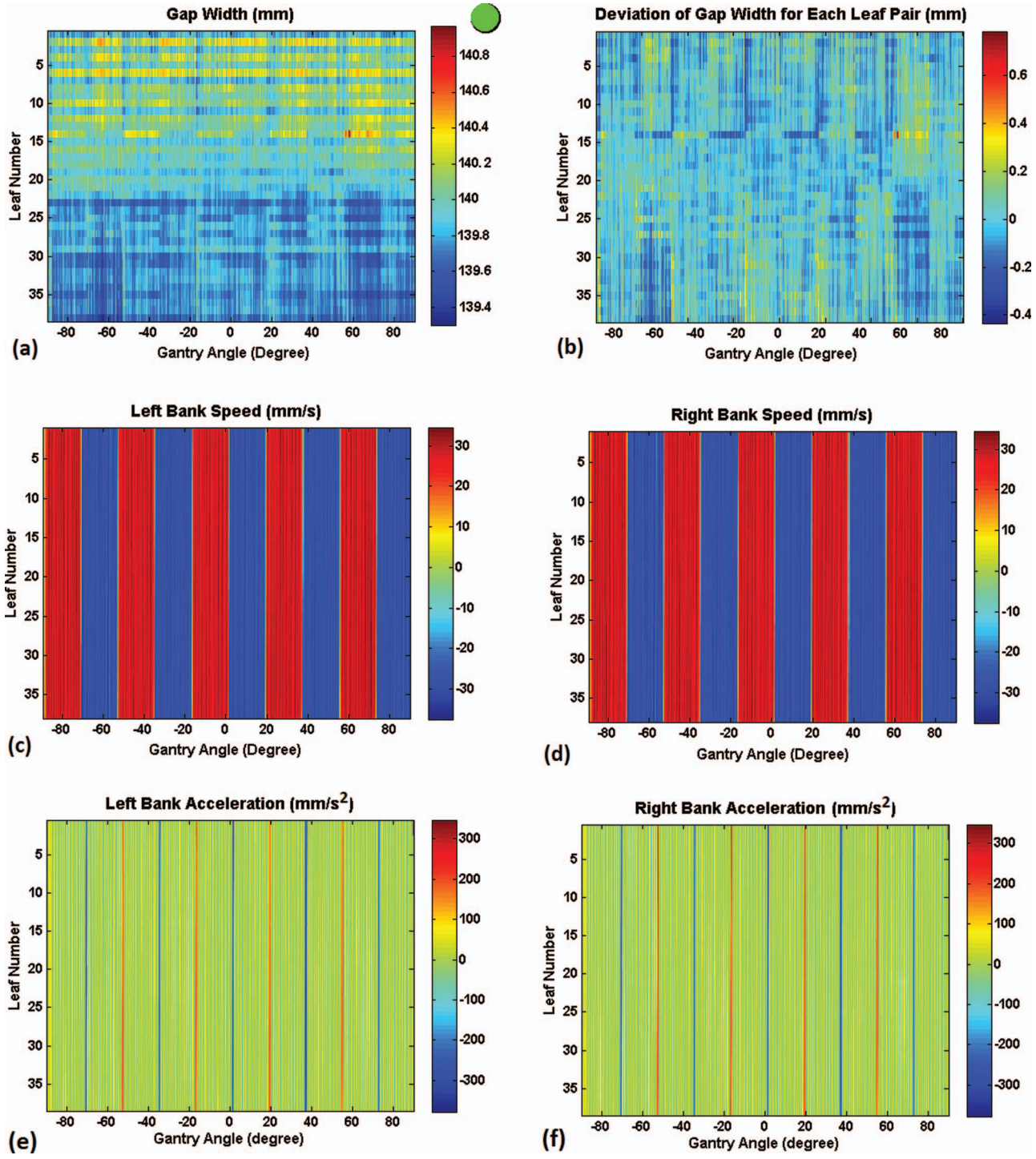

FIG. 7. The graphical output sheet for the analysis of a 140 mm sliding gap traveling back and forth across the field in arc delivery mode: (a) the gap width pattern for different gantry angles; (b) deviation of the gap widths from the average of gap widths defined by the corresponding leaf pair across the field; (c) the speed of each leaf in the left bank (left to right movement is considered as the positive direction); (d) the speed of each leaf in the right bank; (e) the acceleration/deceleration of each leaf in the left bank; and (f) the acceleration/deceleration of each leaf in the right bank.

Table IV shows that the gantry rotation does not have a major effect on gap width (up to 0.02 mm). The maximum effect of gantry angle on the deviation of the peak positions from their expected positions (with respect to the beam central axis) was about 0.1 mm. The maximum effect on MLC skewness was ~0.1°. Similar results were obtained for the other two tested linacs.

A similar investigation on gantry angle dependence was performed on DMLC using a unidirectional 5 mm sliding gap traveling at 19.3 mm/s speed. The results are given in Table V.

Table V shows that the RMSD of the measured and nominal gap width was not affected by the gantry rotation by more than 0.02 mm. The maximum deviation from nominal gap

TABLE II. The analysis results for testing the consistency of gap width and leaf speed for a unidirectional 5 mm sliding gap delivered at a fixed gantry angle. The average of three measurements are presented with ±1 SD.

Nominal leaf speed (mm/s)	6.73	9.67	19.33	29.01
Average detected speed (mm/s)	6.73 ± 0.06	9.69 ± 0.21	19.42 ± 0.22	29.17 ± 0.35
Maximum deviation from average leaf speed (mm/s)	0.25 ± 0.01	0.64 ± 0.03	0.92 ± 0.06	1.58 ± 0.06
RMSD between left and right bank speeds (mm/s)	0.10 ± 0.00	0.21 ± 0.00	0.32 ± 0.01	0.49 ± 0.01
Maximum deviation from nominal gap width (mm)	0.22 ± 0.04	0.24 ± 0.06	0.25 ± 0.06	0.35 ± 0.08
RMSD of measured and nominal gap widths (mm)	0.09 ± 0.00	0.09 ± 0.00	0.09 ± 0.00	0.09 ± 0.00

width at different gantry angles were up to 0.3 mm. Changes in the RMSD of the leaf speeds in the left and right banks at different gantry angles were affected by up to 0.1 mm/s. Similar results were obtained for the other two tested linacs.

III.E. Accuracy of the algorithm

Results of the detection of deliberately inserted errors in leaf positions in the picket fence pattern, and the detection of intentional changes made in gap positions are given in Table VI.

The average difference between the nominal and measured shifts in the gap widths and leaf pair positions were both 0.01 mm.

According to Table II, the sliding gap algorithm detected the leaf speed for the range of tested velocities for a unidirectional gap with an average accuracy of 0.07 mm/s. The RMSD of the measured and nominal gap widths across the field was 0.09 mm for all tested leaf speeds.

The detected angles of the rotated image were compared with the applied (nominal) rotation angles. The result was an RMSD of 0.03° which was considered as the accuracy of the Radon transform.

IV. DISCUSSION

In advanced radiotherapy treatments, errors in the width of MLC-defined gaps could lead to inaccurate delivery of the prescribed doses, and errors in the gap position could result in geometric inaccuracies in tumour targeting.[9] Correct MLC positioning is more important for highly modulated IMRT fields[17] and arc treatments,[52] especially for fields with small apertures, or at the edges of the subfields where dose errors are proportional to the penumbra slope.[28] Considering the complexity of IMRT/VMAT treatments, accurate delivery of the prescribed doses requires stable and reliable electromechanical systems which in turn necessitate extensive knowledge of MLC positioning and accurate quality assurance methods. Ideally, the best practice would be to develop simple methods to cover more efficient QA programs. In this study, robust algorithms are developed to extract greater information from some well-known tests by observing the collected measured data from a different point of view, and by adding new tests for more comprehensive investigation of the system.

The picket fence test was used to provide information on leaf positions, gap widths and skewness of the system over the whole range of leaf positions. The distinction of the picket fence test results in the present work compared with previous studies is in finding the deviation of each detected peak position from its expected position with respect to the beam central axis (to find systematic shifts), and also in determination of the system skewness. In addition, the leaf-by-leaf analysis performed in this study provides quantitative data for each individual leaf with sub-pixel accuracy, and the analysis results are presented through several graphs to make it easier for the user to detect the leaf tolerance violations and to quickly review the analysis results. The log files provide a useful source of archived information for long-term investigations of the stability of the MLC performance.

Deviations up to 0.52 mm in gap width and 0.80 mm from the expected peak positions were recorded among three linacs over 5 months of observation. Performing the test in both fixed-gantry (at cardinal angles) and arc modes generalized the QA method to both IMRT and VMAT deliveries. The results with the gantry fixed at cardinal angles showed that the

TABLE III. Summary of the statistical investigation of the results for different tests on the leaf speed. The average of three measurements are presented with ±1 SD.

Test	Delivery mode	Leaf speed (mm/s)	RMSD of measured and nominal gap widths (mm)	Maximum deviation from nominal gap width (mm)	RMSD between left and right bank speeds (mm/s)
Unidirectional gap	Arc	2.02	0.11 ± 0.01	0.39 ± 0.04	0.37 ± 0.05
Bidirectional gap	Static	19.33	0.08 ± 0.01	0.29 ± 0.06	0.48 ± 0.01
Unidirectional gap, different speeds	Static	2.23 to 20.08	0.09 ± 0.00	0.31 ± 0.05	0.39 ± 0.00
Oscillating gap	Arc	27.50	0.21 ± 0.02	0.97 ± 0.08	1.35 ± 0.03

TABLE IV. Comparison of the picket fence results at cardinal angles and during arc delivery. The average data over all leaf pairs are given ± 1 SD. The nominal gap width was 1 mm.

Gantry angle (degrees)	0	90	180	270	Arc
Gap width (mm)	0.99 ± 0.12	0.98 ± 0.13	1.00 ± 0.13	1.00 ± 0.12	0.99 ± 0.10
Deviation from average peak position (mm)	0.01 ± 0.02	0.02 ± 0.02	0.01 ± 0.03	0.03 ± 0.02	0.03 ± 0.02
Deviation from expected peak position (mm)	0.21 ± 0.05	0.23 ± 0.06	0.24 ± 0.15	0.33 ± 0.07	0.30 ± 0.07
MLC skewness (degrees)	− 0.23 ± 0.01	− 0.31 ± 0.00	− 0.21 ± 0.00	− 0.09 ± 0.01	− 0.23 ± 0.01

peak positions were displaced from their expected positions by up to 0.1 mm, while the effect of gravity and friction on the gap widths was negligible. This confirmed the report by Vieira *et al.*[25] It should be emphasized that the EPID and gantry sag effect on the tests performed in arc mode were found to be negligible in the tested linacs and were not considered in this study.

The heavy weight of the MLC assembly results in excessive force imposed on the carriage bearings which may lead to the skewing of the leaf banks.[2,10,53] There is also a possibility of some small EPID skewing relative to the linac head.[7,54] In this study, the overall skewness of the system including the MLC assembly, collimator, and EPID was investigated and the contribution of the MLC system alone was separately evaluated for the tested linacs, which was less than 0.2°. Misalignments up to 1° would only result in negligible change in dose distribution as reported by Bhagwat *et al.*[55] and is in accordance with the AAPM Task Group report 142.[18] If the system exceeds the tolerance levels for skewness or has a large systematic shift in leaf positioning, the results may be attributed to carriage sag and adjustment or replacement of carriage bearings or adjustment of its belt tension may be required. However, the possibility of an error in the calibration procedure should also be considered.

Some leaf positioning errors could be temporarily eliminated by reinitializing the MLC.[2,56] It was shown in this study that 4 h of linac work (after MLC initialization) could affect 3% of the peak positions in a picket fence pattern by a maximum of 0.2 mm and could change 12% of the gap widths by up to 0.4 mm. Therefore, it would be a good idea to reinitialize the MLC every 4 h. It is important to note that errors in the leaf calibration process could be the main cause of systematic errors in leaf banks. These errors are affected by the stability of the infrared source used for MLC calibration.[25,26]

Deliberately inserted errors in leaf positions in a range of 0.1 mm to 2.5 mm as well as changes in the gap positions were detected by the algorithm with an average accuracy of 0.01 mm. These results indicate the superiority of the method used in this work to previous studies which were based on visual inspection of the errors on film or EPID images.

In addition to the picket fence test which evaluates the MLC performance in static leaf positions, a comprehensive QA program would require investigation of the behavior of leaves in dynamic beam deliveries. In this study, assessment of the dynamic MLC performance was based on the evaluation of sliding gaps traveling across the field in different conditions in both gantry-fixed and arc modes. In arc deliveries, gravity and friction between leaves (e.g., due to the accumulation of dirt or grease) may affect the stability of MLC speed during gantry rotation. The sliding gap test is sensitive to small changes in leaf position and speed across the range of leaf travel which could be affected by motor fatigue and lead to changes in the leaf acceleration/deceleration.[1,9]

Using the EPID in cine imaging mode provides an opportunity to analyze the images of a sliding gap as time-lapse series. Thus, another dimension was added to the results and changes in the gap widths, leaf speeds, and leaf acceleration/deceleration could be examined. This is a major advantage over film measurements. It must be noted that movements of the gantry and imager during the delivery are not expected to cause blurring at the edge of images since only one frame is used per image.[30,32]

The accuracy and precision of leaf positioning is slightly reduced for higher leaf speed deliveries. This finding is in accordance with previous studies.[28,36] The leaf speed for a unidirectional gap in arc mode was lower than the fixed-gantry setup, since the aim was to perform the test in an entire 360° arc delivery while the maximum gantry speed is limited to 5° per second. However, the gap width and leaf speeds were both affected by gravity during arc delivery. The change in the direction of leaf travel in a bidirectional gap in fixed-gantry condition resulted in an increase in the RMSD between the speeds of corresponding leaves in the left and right banks compared with a unidirectional sliding gap moving with the same leaf speed. Application of speed gradients to the unidirectional sliding gap (average speed ∼10 mm/s) led to larger

TABLE V. Comparison of the results of the unidirectional 5 mm sliding gap test at cardinal angles and during arc delivery. The average of three measurements is presented with ±1 SD.

Gantry angle (degrees)	0	90	180	270	Arc
RMSD of measured and nominal gap widths (mm)	0.09 ± 0.00	0.09 ± 0.00	0.12 ± 0.00	0.10 ± 0.00	0.11 ± 0.00
Maximum deviation from nominal gap width (mm)	0.25 ± 0.06	0.29 ± 0.04	0.31 ± 0.05	0.55 ± 0.07	0.42 ± 0.04
RMSD between left and right bank speeds (mm/s)	0.32 ± 0.01	0.34 ± 0.03	0.37 ± 0.01	0.40 ± 0.04	0.39 ± 0.05

TABLE VI. Results of the algorithm for detection of the intentionally inserted errors in the picket fence pattern and in the gap positions. The average of three measurements is presented with ±1 SD.

Nominal inserted shift (mm)	0.1	0.2	0.3	0.5	0.7	1.5	2	2.5
Detected change in gap width (mm)	0.11 ± 0.02	0.20 ± 0.03	0.31 ± 0.02	0.52 ± 0.01	0.69 ± 0.02	1.50 ± 0.01	2.01 ± 0.02	2.49 ± 0.02
Detected change in leaf pair position (mm)	0.10 ± 0.00	0.21 ± 0.02	0.31 ± 0.02	0.51 ± 0.01	0.70 ± 0.01	1.49 ± 0.02	2.00 ± 0.03	2.50 ± 0.01

differences between the nominal and measured gap widths and larger RMSD between the speeds of corresponding leaves in the left and right banks when compared to a gap traveling with a constant speed of 9.67 mm/s. The results for the oscillating gap test had the largest deviations and RMSDs, as expected. Although the test conditions are extremely stringent and are unlikely to be applied in clinical practice, it is a suitable test for QA purposes.

The accepted tolerance for deviation of leaf speed from its nominal value was ±5 mm/s in this study, based on the AAPM Task Group report 142.[18] However, in the most difficult test conditions (oscillating gap during arc with high speed), the maximum deviation of leaf speeds from the nominal value was less than 3 mm/s.

The tests performed in this study in conjunction with the algorithms could be included in the routine QA tests as part of the MLC maintenance procedures for IMRT/VMAT to identify problems with MLC motors before they become clinically significant. The MLC interlock is usually activated at 2 mm leaf positioning error[5,8,14,57] to avoid unacceptable number of beam interruptions.[8,36] Therefore, much tighter tolerances are required for the QA of IMRT/VMAT. Jorgensen *et al.*[7] have proposed 0.3 mm and 0.5 mm tolerance levels for leaf positioning and gap width errors in VMAT QA which seem reasonable based on the results of this study.

Leaving a slow moving leaf unchanged could finally lead to its getting stuck during a treatment session.[9] Based on the results of this study, considering the quick test procedure and the short algorithm processing times, a timetable is suggested for the MLC QA tests as scheduled in Table VII. The daily picket fence test after the last treatment helps in identification of the faulty motors more easily due to the longer time elapsed since the last MLC re-initialization. It is also necessary to perform the picket fence test after any changes to the optical system for MLC calibration.

TABLE VII. The suggested timetable for MLC performance tests for IMRT/VMAT based on the present study.

Test	Fixed gantry angles	Arc	At cardinal angles
Picket fence	• Daily, after machine warm-up • Daily, after the last treatment • Before patient specific QA	Weekly	Monthly
Unidirectional sliding gap	Daily	Weekly	Monthly
Other sliding gap tests	Monthly	Monthly	Monthly

After changing a leaf motor it would be required to check its performance by carrying out a picket fence test and a unidirectional sliding gap test at fixed gantry angles.

It must be noted that comprehensive QA for VMAT treatments requires two other tests. These tests were introduced by Ling *et al.*[22] and include investigation of the effects of varying dose rate/gantry speed, and varying dose rate/MLC speed. EPID images can be used for these tests as addressed by Jorgensen *et al.*[7]

V. CONCLUSION

This study provides convenient test methods for routine QA of the MLC performance as well as troubleshooting of the MLC problems in both IMRT and VMAT treatments. The fast, easy, and accurate measurement methods and the robust algorithms introduced in this study help in performing the tests more frequently and therefore improve the clinical outcomes. The large amounts of information shown on several graphs enable the physicists to have immediate access to many quantities which could help finding the problems by looking at them from various aspects and decision making on selection of the most convenient rectification strategy.

ACKNOWLEDGMENTS

This work was supported by the National Health and Medical Research Council (Grant No. 569211). The authors wish to thank Dr. Kym Nitschke and Mr. Todsaporn Fuangrod for their helpful remarks. P. R. gratefully acknowledges the award of the UNIPRS scholarship from the University of Newcastle, Australia.

[a]Author to whom correspondence should be addressed. Electronic mail: Pejman.Rowshanfarzad@uon.edu.au; Telephone: +61249211869; Fax: +61249211138.

[1]T. LoSasso, Ch. Chui, and C. C. Ling, "Physical and dosimetric aspects of a multileaf collimation system used in the dynamic mode for implementing intensity modulated radiotherapy," Med. Phys. **25**, 1919–1927 (1998).
[2]T. LoSasso, Ch. Chui, and C. C. Ling, "Comprehensive quality assurance for the delivery of intensity modulated radiotherapy with a multileaf collimator used in the dynamic mode," Med. Phys. **28**, 2209–2219 (2001).
[3]C. X. Yu, "Intensity-modulated arc therapy with dynamic multileaf collimation: An alternative to tomotherapy," Phys. Med. Biol. **40**, 1435–1449 (1995).

[4]K. Otto, "Volumetric modulated arc therapy: IMRT in a single gantry arc," Med. Phys. **35**, 310–317 (2008).
[5]A. Rangel, and P. Dunscombe, "Tolerances on MLC leaf position accuracy for IMRT delivery with a dynamic MLC," Med. Phys. **36**, 3304–3309 (2009).
[6]P. Rowshanfarzad, M. Sabet M, D. J. O'Connor, and P. B. Greer, "Investigation of the sag in linac secondary collimator and MLC carriage during arc deliveries," Phys. Med. Biol. **57**(12), N209–N224 (2012).
[7]M. K. Jørgensen, L. Hoffmann, J. B. B. Petersen, L. H. Præstegaard, R. Hansen, and L. P. Muren, "Tolerance levels of EPID-based quality control for volumetric modulated arc therapy," Med. Phys. **38**(3), 1425–1434 (2011).
[8]D. W. Litzenberg, J. M. Moran, and B. A. Fraass "Incorporation of realistic delivery limitations into dynamic MLC treatment delivery," Med. Phys. **29**(5), 810–820 (2002).
[9]T. Losasso, "IMRT delivery performance with a Varian multileaf collimator," Int. J. Radiat. Oncol., Biol., Phys. **71**(1), S85–S88 (2008).
[10]C. D Mubata, P. Childs, and A. M. Bidmead, "A quality assurance procedure for the Varian multi-leaf collimator," Phys. Med. Biol. **42**, 423–431 (1997).
[11]P. Xia, C. F. Chuang, and L. J. Verhey, "Communication and sampling rate limitations in IMRT delivery with a dynamic multileaf collimator system," Med. Phys. **29**(3), 412–423 (2002).
[12]J. Chang, C. H. Obcemea, J. Sillanpaa, J. Mechalakos, and C. Burman, "Use of EPID for leaf position accuracy QA of dynamic multi-leaf collimator (DMLC) treatment," Med. Phys. **31**, 2091–2096 (2004).
[13]I. Chauvet, A Petitfils, C. Lehobey, J. K. Kristner, Y. Brunet, R. Lembrez, G. Gaboriaud, A. Mazal, S. Zefkili, and J. C. Rosenwald "The sliding slit test for dynamic IMRT: A useful tool for adjustment of MLC related parameters," Phys. Med. Biol. **50**, 563–580 (2005).
[14]W. Luo, J. Li, R. A. Price, L. Chen, J. Yang, J. Fan, Z. Chen, S. McNeeley, X. Xu, and C. M. Ma, "Monte Carlo based IMRT dose verification using MLC log files and R/V outputs," Med. Phys. **33**, 2557–2564 (2006).
[15]J. Richart, M. C. Pujades, J. Perez-Calatayud, D. Granero, F. Ballester, S. Rodriguez, and M. Santos, "QA of dynamic MLC based on EPID portal dosimetry," Physica Medica: Eur. J. Med. Phys. **28**(3), 262–268 (2012).
[16]A. Rangel, G. Palte, and P. Dunscombe, "The sensitivity of patient specific IMRT QC to systematic MLC leaf bank offset errors," Med. Phys. **37**(7), 3862–3867 (2010).
[17]G. J. Budgell, J. H. Mott, P. C. Williams, and K. J. Brown, "Requirements for leaf position accuracy for dynamic multileaf collimation," Phys. Med. Biol. **45**, 1211–1227 (2000).
[18]E. E. Klein, J. Hanley, and J. Bayouth, "Task Group 142 report: Quality assurance of medical accelerators," Med. Phys. **36**, 4197–4212 (2009).
[19]M. Alber, *et al.*, *ESTRO Booklet No.9: Guidelines for the Verification of IMRT* (ESTRO, Brussels, Belgium, 2008).
[20]C. S. Chui, S. Spirou, and T. LoSasso "Testing of dynamic multileaf collimation," Med. Phys. **23**(5), 635–641 (1996).
[21]M. L. P. Dirkx and B. J. M. Heijmen, "Testing of the stability of intensity modulated beams generated with dynamic multileaf collimation, applied to the MM50 racetrack microtron," Med. Phys. **27**(12), 2701–2707 (1997).
[22]C. C. Ling, P. Zhang, Y. Archambault, J Bocanek, G. Tang, and T. Losasso, "Commissioning and quality assurance of rapidarc radiotherapy delivery system," Int. J. Radiat. Oncol., Biol. Phys. **72**(2), 575–581 (2008).
[23]C. D. Venencia, and P. Besa, "Commissioning and quality assurance for intensity modulated radiotherapy with dynamic multileaf collimator: Experience of the Pontificia Universidad Católica de Chile," J. Appl. Clin. Med. Phys. **5**(3), 37–54 (2004).
[24]D. S. Sharma, P. M Dongre, V. Mhatre, and M. Heigrujam "Physical and dosimetric characteristic of high-definition multileaf collimator (HDMLC) for SRS and IMRT," J. Appl. Clin. Med. Phys. **12**(3), 142–160 (2011).
[25]S. C. Vieira, M. L. P. Dirkx, K. L. Pasma, and B. J. M. Heijmen "Fast and accurate leaf verification for dynamic multileaf collimation using an electronic portal imaging device," Med. Phys. **29**(9), 2034–2040 (2002).
[26]C. Vieira, R. A. Bolt, M. L. P. Dirkx, A. G. Visser, and B. J. M. Heijmen "Fast, daily linac verification for segmented IMRT using electronic portal imaging," Radiother. Oncol. **80**, 86–92 (2006).
[27]S. J. K. Baker, G. J. Budgell, and R. I. MacKay, "Use of an amorphous silicon electronic portal imaging device for multileaf collimator quality control and calibration" Phys. Med. Biol. **50**, 1377–1392 (2005).
[28]D. A. Low, J. W. Sohn, E. E. Klein, J. Markman, S. Mutic, and J. F. Dempsey, "Characterization of a commercial multileaf collimator used for intensity modulated radiation therapy," Med. Phys. **28**, 752–756 (2001).
[29]S. S. Samant, W. Zheng, N. A. Parra, J. Chandler, A. Gopal, J. Wu, J. Jain, Y. Zhu, and M. Sontag, "Verification of multileaf collimator leaf positions using an electronic portal imaging device," Med. Phys. **29**, 2900–2912 (2002).
[30]H. V. James, S. Atherton, G. J. Budgell, M. C. Kirby and P. C. Williams, "Verification of dynamic multileaf collimation using an electronic portal imaging device," Phys. Med. Biol. **45**, 495–509 (2000).
[31]O. A. Zeidan, J. G. Li, M. Ranade, A. M. Stell, and J. F. Dempsey,"Verification of step-and-shoot IMRT delivery using a fast video-based electronic portal imaging device" Med. Phys. **31**(3), 463–476 (2004).
[32]J. J. Sonke, L. S. Ploeger, B. Brand, M. H. Smitsmans, and M. van Herk, "Leaf trajectory verification during dynamic intensity modulated radiotherapy using an amorphous silicon flat panel imager," Med. Phys. **31**(2), 389–395 (2004).
[33]X. Mei, I. Nygren, and J. E. Villarreal-Barajas, "On the use of the MLC dosimetric leaf gap as a quality control tool for accurate dynamic IMRT delivery" Med. Phys. **38**(4), 2246–2255 (2011).
[34]J. G. Li, J. F. Dempsey, L. Ding, C. Liu, and J. R. Palta, "Validation of dynamic MLC-controller log files using a two-dimensional diode array," Med. Phys. **30**(5),799–805 (2003).
[35]D. Moreno, D. Venencia, E. Garrigo, and Y. Pipman, "A method to enhance spatial resolution of a 2D ion chamber array for quality control of MLC," J. Appl. Clin. Med. Phys. **12**(4), 63–73 (2011).
[36]P. Zygmanski, J. H. Kung, S. B. Jiang, and L. Chin, "Dependence of fluence errors in dynamic IMRT on leaf-positional errors varying with time and leaf number" Med. Phys. **30**(10), 2736–2749 (2003).
[37]M. Stell, J. G. Li, O. A. Zeidan, and J. F. Dempsey, "An extensive log-file analysis of step-and-shoot intensity modulated radiation therapy segment delivery errors," Med. Phys. **31**(6),1593–1602 (2004).
[38]M. Okumura, Y. Obata, K. Shimomura, M. Tamura and Y. Nishimura, "The effect of gantry and collimator angles on leaf limited velocity and position in dynamic multileaf collimator intensity-modulated radiation therapy," Phys. Med. Biol. **55**, 3101–3113 (2010).
[39]K. Wijesooriya, C. Bartee, J. V. Siebers, S. S. Vedam, and P. J. Keall, "Determination of maximum leaf velocity and acceleration of a dynamic multileaf collimator: Implications for 4D radiotherapy," Med. Phys. **32**, 932–941 (2005).
[40]International Electrotechnical Commission (IEC), "Radiotherapy equipment: Coordinates, movements and scales," Report No. IEC 61217 (IEC, Geneva, 2008).
[41]https://my.varian.com/.
[42]P. Rowshanfarzad, M. Sabet, D. J. O'Connor, P. M. McCowan, B. M. C. McCurdy, and P. B. Greer, "Detection and correction for EPID and gantry sag during arc delivery using cine EPID imaging," Med. Phys. **39**(2), 623–635 (2012).
[43]J. Canny, "A computational approach to edge detection", IEEE Trans. Pattern Anal. Mach. Intell. **8**, 679–698 (1986).
[44]P. Rowshanfarzad, M. Sabet, D. J. O'Connor, and P. B. Greer, "Verification of the linac isocentre for stereotactic radiosurgery using cine-EPID imaging and arc delivery," Med. Phys. **38**(7), 3963–3970 (2011).
[45]L. Clews and P. B. Greer, "An EPID based method for efficient and precise asymmetric jaw alignment quality assurance," Med. Phys. **36**(12), 5488–5496 (2009).
[46]P. B. Greer, P. Cadman, C. Lee, and K. Bzdusek, "An energy fluence-convolution model for amorphous silicon EPID dose prediction," Med. Phys. **36**(2), 547–555 (2009).
[47]Z. Gao, J. Szanto, and L. Gerig, "Using multileaf collimator interleaf leakage to extract absolute spatial information from electronic portal imaging device images," J. Appl. Clin. Med. Phys. **8**(1), 1–9 (2007).
[48]A. Boyer, P. Biggs, J. Galvin, E. Klein, T. LoSasso, D. Low, K. Mah, and C. Yu, "Basic applications of multileaf collimators," Report of the AAPM Radiation Therapy Committee Task Group No. 50 (Medical Physics Publishing, 2001).
[49]M. N. Graves, A. V. Thompson, M. K. Martel, D. L. McShan, and B. A. Fraass, "Calibration and quality assurance for rounded leaf-end MLC systems," Med. Phys. **28**(11), 2227–2233 (2001).

[50]G. A. Ezzell, J. M. Galvin, D. Low, J. R. Palta, I. Rosen, M. B. Sharpe, P. Xia, Y. Xiao, L. Xing, and C. X. Yu, "Guidance document on delivery, treatment planning, and clinical implementation of IMRT: Report of the IMRT subcommittee of the AAPM radiation therapy committee" Med. Phys. **30**(8), 2089–2115 (2003).
[51]P. Vial, L. Oliver, P. B. Greer, and C. Baldock, "An experimental investigation into the radiation field offset of a dynamic multileaf collimator," Phys. Med. Biol. **51**, 5517–5538 (2006).
[52]A. Van Esch, D. P. Huyskens, C. F. Behrens, E. Samsøe, M. Sjölin, U. Bjelkengren, D. Sjöström, C. Clermont, L. Hambach, and F. Sergent, "Implementing RapidArc into clinical routine: A comprehensive program from machine QA to TPS validation and patient QA," Med. Phys. **38**(9), 5146–5166 (2011).
[53]E. E. Klein, W. B. Harms, D. A. Low, V. Willcut, and J. A. Purdy, "Clinical implementation of a commercial multileaf collimator: Dosimetry, networking, simulation, and quality assurance," Int. J. Radiat. Oncol., Biol. Phys. **33**, 1195–1208 (1995).
[54]A. Fredh, S. Korreman, and P. Munck af Rosenschöld, "Automated analysis of images acquired with electronic portal imaging device during delivery of quality assurance plans for inversely optimized arc therapy," Radiother. Oncol. **94**, 195–198 (2010).
[55]M. S. Bhagwat, Z. Han, S. K. Ng, and P. Zygmanski, "An oscillating sweeping gap test for VMAT quality Assurance," Phys. Med. Biol. **55**, 5029–5044 (2010).
[56]E. Bayouth, D. Wendt, and S. M. Morrill, "MLC quality assurance techniques for IMRT applications," Med. Phys. **30**, 743–750 (2003).
[57]G. Mu, E. Ludlum, and P. Xia, "Impact of MLC leaf position errors on simple and complex IMRT plans for head and neck cancer," Phys. Med. Biol. **53**, 77–88 (2008).